



X-RAY RESONANT RAMAN SCATTERING

SPECTRA SIMULATION FROM FIRST PRINCIPLES
FOR COPPER BELOW IONIZATION THRESHOLD
USING HIGH-PERFORMANCE COMPUTING

GONÇALO GARCÊS SOBREIRA RODRIGUES BAPTISTA

BSc in Physics Engineering

DOCTORATE IN PHYSICS ENGINEERING

NOVA University Lisbon
September, 2023

X-RAY RESONANT RAMAN SCATTERING

SPECTRA SIMULATION FROM FIRST PRINCIPLES
FOR COPPER BELOW IONIZATION THRESHOLD
USING HIGH-PERFORMANCE COMPUTING

GONÇALO GARCÊS SOBREIRA RODRIGUES BAPTISTA

BSc in Physics Engineering

Advisers: Jorge Felizardo Machado
Auxiliary Professor, NOVA University Lisbon
Mauro António Guerra
Auxiliary Professor, NOVA University Lisbon

Examination Committee

Chair: Name of the committee chairperson
Full Professor, FCT-NOVA

Rapporteur: Name of a rapporteur
Associate Professor, Another University

Members: Another member of the committee
Full Professor, Another University
Yet another member of the committee
Assistant Professor, Another University

DOCTORATE IN PHYSICS ENGINEERING

NOVA University Lisbon

September, 2023

X-ray resonant Raman scattering

Spectra simulation from first principles for Copper bellow ionization threshold using high-performance computing

Copyright © Gonalo Garcês Sobreira Rodrigues Baptista, NOVA School of Science and Technology, NOVA University Lisbon.

The NOVA School of Science and Technology and the NOVA University Lisbon have the right, perpetual and without geographical boundaries, to file and publish this dissertation through printed copies reproduced on paper or on digital form, or by any other means known or that may be invented, and to disseminate through scientific repositories and admit its copying and distribution for non-commercial, educational or research purposes, as long as credit is given to the author and editor.

Acknowledgements

Acknowledgments are personal text and should be a free expression of the author.

However, without any intention of conditioning the form or content of this text, I would like to add that it usually starts with academic thanks (instructors, etc.); then institutional thanks (Research Center, Department, Faculty, University, FCT / MEC scholarships, etc.) and, finally, the personal ones (friends, family, etc.).

But I insist that there are no fixed rules for this text, and it must, above all, express what the author feels.

”

*“Sometimes I’ll start a sentence, and I don’t even know where it’s going.
I just hope I find it along the way.
Like an improv conversation.
An improversation.”*

— **Michael Scott**, *The Office*
(Regional Manager of Dunder Mifflin Scranton)

”

all work and no play makes Jack a dull boy

[illegible]

— **Jack Torrance**, *The Shinning*
(Caretaker of the Overlook)

Abstract

The work performed on this thesis comes as part of the effort to further understand the highly convoluted structure present on Copper's X-ray emission spectra, where, as with many other transition metals, a skewness can be observed on the $K_{\alpha_{1,2}}$, K_{β} and L transition lines. These lines originate due to the radiative relaxation of the atom's electronic structure post-ionization of inner shell electrons. However, it is very likely that the observed skewness is due to copper's satellite states' transitions.

Throughout this thesis, a study will be performed for the satellite states formed by the excitation of the inner-shell electrons, where, as opposed to the ionization process, usually considered in X-ray calculations, a photoexcitation process occurs.

Multiple atomic structure calculations will be performed using the *ab initio* state of the art [Multiconfiguration Dirac-Fock General Matrix Elements \(MCDFGME\)](#) code for different excited states configurations.

The obtained results will then be used in the analysis of experimental data obtained from a High-Precision [Double Crystal Spectrometer \(DCS\)](#), using a synchrotron X-ray source.

Due to the complexity of the calculations, the process can become substantial in terms of computational power and time. Therefore, further similar and more complex studies will be performed by implementing and running a script in the *Oblivion* supercomputer located at the University of Évora.

Keywords: Atomic Excitation, X-ray lines, [MCDFGME](#), [DCS](#), High Performance Computing

Resumo

asdasdasdasd

Contents

List of Figures	x
List of Tables	xi
Listings	xii
Glossary	xiii
Acronyms	xiv
1 Theoretical Introduction	2
1.1 Characteristic X-rays	2
1.1.1 Ionization as a vacancy generator	2
1.1.2 Transition notation	4
1.1.3 Excitation as a vacancy generator	4
1.2 Radiative transitions	5
1.3 Solving the atomic many-body problem	6
1.3.1 The non-relativistic Hamiltonian	6
1.3.2 The Hartree-Fock Method	7
1.3.3 The Dirac Equation	8
1.4 Quantum Electrodynamics (QED) considerations	11
1.4.1 The Multiconfiguration Dirac-Fock (MCDF) Method	11
1.5 State of the Art	12
1.5.1 Copper's characteristic X-rays	12
1.5.2 MCDFGME capabilities	13
2 Atomic Structure Calculations	14
2.1 The non-relativistic Hamiltonian	14
2.1.1 The Hartree-Fock Method	14
2.2 The Dirac Equation	15

2.3 The Dirac-Breit Equation	18
2.4 The <i>MCDF</i> Method	18
Bibliography	20
Appendices	
A The Breit Hamiltonian Operators	24
B Transition Diagram	26
C QED considerations	27
C.1 Self-Energy	27
C.2 Vacuum Polarization	27
Annexes	
I Input File .f05 Example	28

List of Figures

1.1	Photoionization.	3
1.2	Principal atomic relaxation processes.	3
1.3	Resonant Photoexcitation	5
1.4	HF method's block diagram.	8
1.5	Comparison of Hydrogen level diagrams. Adapted from [13]	12
2.1	HF method's block diagram.	16
B.1	Transition notation scheme. Adapted from [2]	26
C.1	QED Feynman Diagrams	27

List of Tables

1.1 Siegbahn VS IUPAC notation. Adapted from [2].	5
-----------------------------------------------------------	---

Listings

Glossary

Feynman Diagram	2D diagram depicting various physical interactions between elementary particles. Fermions are depicted as straight lines and bosons as wavy lines. (p. 27)
four-vector	Vector used in special relativity composed of 4 components, one scalar time-like, and three vectorial space-like. These vectors behave in special way, such as their norm being Lorentz invariant . Can be written in covariant, X_μ , and contravariant form, X^μ , with the difference being the sign of the time-like components. Example of a contravariant four vector: $X^\mu = (X^0, X^1, X^2, X^3) = (X^0, \mathbf{X})$ (pp. xiii , 9 , 15)
Lorentz invariant	A Lorentz invariant scalar, obtained, for example, from a Minkowski norm , does not change when operated by a Lorentz Transformation. (pp. xiii , 9 , 15)
Minkowski norm	Yields the Lorentz Invariant norm for a four-vector : $p_\mu p^\mu$. Equivalent to the dot product of a classical vector. (pp. xiii , 9 , 15)
self consistency method	The electron wavefunctions go through a variational process in order to reach convergence for an energetic minimum. (p. 7)
virtual photons	While in reality, during a Coulomb interaction, 'real' particles are not exchanged, the electromagnetic field is still mediated by photons. This way virtual photons are tools used in order to better represent electromagnetic interactions. (pp. 11 , 18)

Acronyms

<i>Grasp2k</i>	General-purpose Relativistic Atomic Structure Package 2k (p. 13)
<i>MCDFGME</i>	Multiconfiguration Dirac-Fock General Matrix Elements (pp. vi , 12 , 13 , 18)
<i>MCDF</i>	Multiconfiguration Dirac-Fock (pp. viii , ix , 11 , 18 , 19)
DCS	Double Crystal Spectrometer (p. vi)
EMF	Electromagnetic Field (pp. 6 , 11)
FAC	Flexible Atomic Code (p. 13)
HF	Hartree-Fock (p. 8)
QED	Quantum Electrodynamics (pp. viii , 2 , 11)

Todo list

Figure: Maybe put a Thomas model plot?	4
Explain antisymmetry and put it in the glossary	7
Explain in the glossary	7
Finish the explanation	8
Try to explain why this might be a problem	9
do the demonstration, dummy	9
Falar aqui sobre as contribuições. Não tem que ser extensivo	11
Ler bem o manual e explicar bem o método e todas as coisas diferentes que se podem fazer	11
This really needs a re-do	12

Theoretical Introduction

Throughout this thesis, different topics regarding Quantum Mechanics, Atomic Physics and spectroscopy will be approached, hence why a theoretical introduction is needed. In it, themes such as the characteristic X-rays of elements, the relativistic Dirac equation and QED corrections and methods for solving the many-body problem will be discussed.

1.1 Characteristic X-rays

When subjected to a high energy beam of particles (usually photons or electrons), an element may go through the process of the ionization of inner-core electrons, which is followed by the emission of radiation of its own, in the form of X-rays and/or Auger electrons. The radiation emitted throughout this process presents well-defined energy values and thus provides a way to ascertain if an element is present in a sample under study. Due to this reason, these characteristic emissions are of an extremely high importance in a wide range of scientific areas.

When an atomic system is in a bound state, the electrons orbiting the nucleus are occupying fixed quantum states, defined by their principal atomic number, n , angular momentum, l , and spin, s . Electrons are also fermions, and thus must respect Pauli's exclusion principle, each occupying a single state, only occupied by that single electron. These quantum numbers provide information about each electron's wavefunction, and the collection of all the electrons' wavefunctions can be used in order to describe the whole system. When operating the Hamiltonian on this collection of wavefunctions, the atomic system's state's energy is obtained. Besides all the occupied states, an infinite more number of possible eigenfunctions will compose that system's base.

1.1.1 Ionization as a vacancy generator

As previously mentioned, X-ray fluorescence spectroscopy has many uses and applications in a wide range of scientific areas. In this form of spectroscopy, the element at study, composed of a nucleus and N orbiting electrons, is bombarded with radiation leading to the ionization of inner-shell electrons while leaving a vacancy in their place (Figure 1.1).

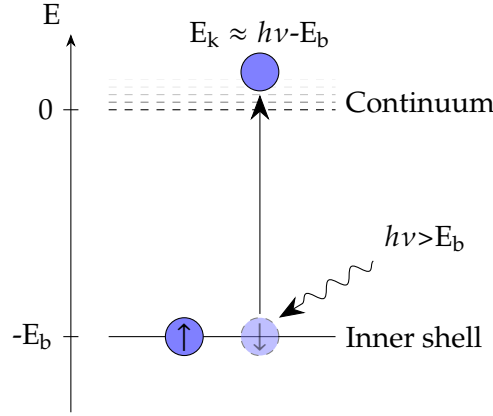


Figure 1.1: Photoionization.

The atomic structure, now composed of $N - 1$ electrons, will be left in an energetically unstable state, due to there being other possible lower energy states. This will lead to various processes of atomic relaxation, where the system will rearrange itself in order to find a lower energy configuration.

The main processes for this rearrangement are two competing decay paths: radiative relaxation, and Auger electron emission.

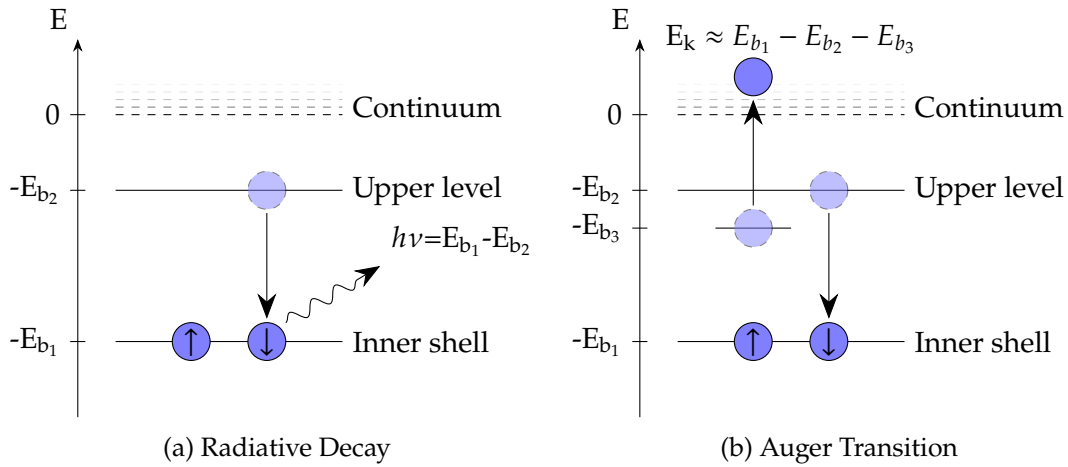


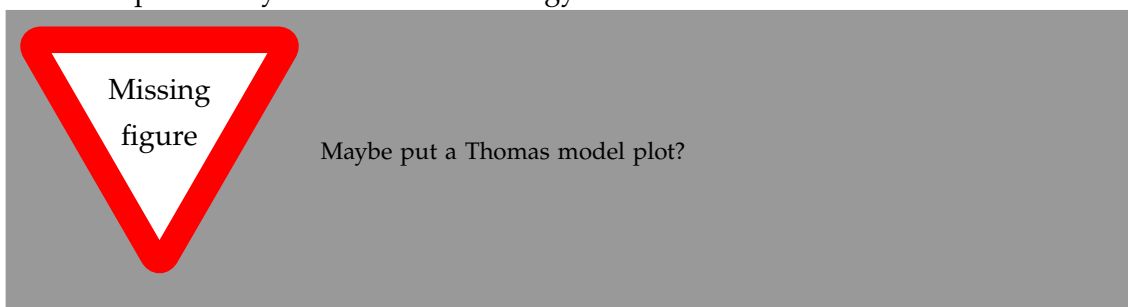
Figure 1.2: Principal atomic relaxation processes.

In the case of radiative relaxation, an upper shell electron will move and occupy the hole left in the inner shell. During this process, energy is released through the emission of photons with energy in the range of X-rays. The detection of these photons is what allows for an analysis and detection of the element at study.

On the other hand, an Auger emission occurs when in the process of an upper electron shifting to a shell hole, energy is released not in the form of photons, but by the atomic system going through the process of the ionization of a lesser bound electron.

In reality, when the initial vacancy is generated, two more processes can occur: shake-off and shake-up. Due to a sudden change in the potential felt by the remaining electrons,

whilst going through the ionization, one other electron may become unbound, leading to a second ionization, the shake-off process, or may be excited to an upper state, during shake-up. These processes' occurrence probabilities are related to the rate at which the electron leaves the system during the first ionization. For lower electron emission energies, where the ionization process is rather "slow", and there is not much energy for shake up/off to occur, the adiabatic regime reigns. In this regime, the shake probabilities are small, and increase with the beam's energy. For higher energies, the transition occurs in the sudden regime, where the electrons' exit can be considered instantaneous. Now, while the shake probabilities still increase with the energy of the beam, they quickly saturate for a maximum value of probability, which can be calculated by computing overlaps between the electrons' initial and final states. These processes, however, are out of scope for this thesis, but should the reader be interested, the model conceived by Thomas [1] predicts the shake probability as a function of energy.



1.1.2 Transition notation

The characteristic radiation measured from the radiative relaxation of a post-ionization unstable atomic system is one of the main ways of identifying an atomic element. This is due to the photons emitted possessing quantized values of energy, forming well-defined energy lines when observed in a spectrometer. In order to understand the change that occurred in the atomic system which lead to a specific emission, the spectral lines get labels based on a notation which usually takes into account the initial and final orbitals where the vacancy was present. A very illustrative diagram, exemplifying some transitions can be found in Appendix B.

Throughout this thesis, Siegbahn notation will be used, for the most part, but should the reader prefer IUPAC's, Table 1.1 has the conversion between notations.

1.1.3 Excitation as a vacancy generator

As previously mentioned, throughout this thesis, while the study is focused on the characteristic radiation emitted during an atomic relaxation process, the main vacancy generation method at study shall be the photoexcitation process (Figure 1.3), instead of ionization. The levels obtained after a photoexcitation of core shell electrons has occurred could be some of the many so-called satellite states, where the electronic configuration present during the relaxation process contains additional electrons or holes, or is simply not

Table 1.1: Siegbahn VS IUPAC notation. Adapted from [2].

Siegbahn	IUPAC	Siegbahn	IUPAC	Siegbahn	IUPAC
K_{α_1}	$K - L_3$	L_{α_1}	$L_3 - M_5$	L_{γ_1}	$L_2 - N_4$
K_{α_2}	$K - L_2$	L_{α_2}	$L_3 - M_4$	L_{γ_2}	$L_1 - N_1$
K_{β_1}	$K - M_3$	L_{β_1}	$L_2 - M_4$	L_{γ_3}	$L_1 - N_2$
$K_{\beta_2}^I$	$K - N_3$	L_{β_2}	$L_3 - N_5$	L_{γ_4}	$L_1 - O_3$
$K_{\beta_2}^{II}$	$K - N_2$	L_{β_3}	$L_1 - M_3$	L_{γ_4}'	$L_1 - O_2$
K_{β_3}	$K - M_2$	L_{β_4}	$L_1 - M_2$	L_{γ_5}	$L_2 - N_1$
$K_{\beta_4}^I$	$K - N_5$	L_{β_5}	$L_3 - O_{4,5}$	L_{γ_5}'	$L_2 - O_4$
$K_{\beta_4}^{II}$	$K - N_4$	L_{β_6}	$L_3 - N_1$	L_{γ_8}	$L_2 - O_1$
$K_{\beta_4}^x$	$K - N_4$	L_{β_7}	$L_3 - O_1$	L_{γ_8}'	$L_2 - N_{5,6}$
$K_{\beta_5}^I$	$K - M_5$	L_{β_8}	$L_3 - N_{6,7}$	L_{η}	$L_2 - M_1$
$K_{\beta_4}^{II}$	$K - M_4$	L_{β_9}	$L_1 - M_5$	L_l	$L_3 - M_1$
		L_{β_9}	$L_1 - M_4$	L_s	$L_3 - M_3$
		L_{β_9}	$L_3 - N_4$	L_t	$L_3 - M_2$
		L_{β_9}	$L_2 - M_3$	L_u	$L_3 - N_{6,7}$
				L_v	$L_2 - N_{6,7}$

the standard configuration when talking about characteristic emissions. The characteristic radiation from transitions that originated from these states are one of the keys needed to fully comprehend and deconvolute an element's emission spectra.

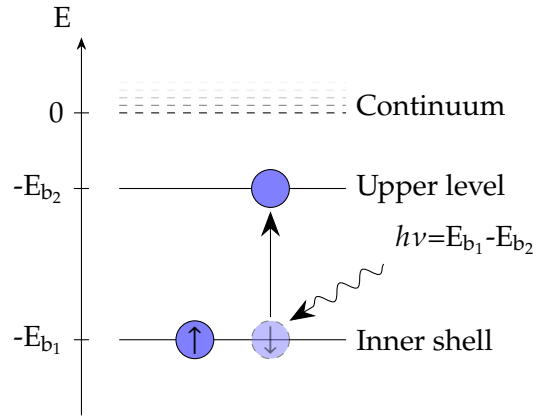


Figure 1.3: Resonant Photoexcitation

1.2 Radiative transitions

In terms of quantum mechanics, the properties of a system's change of state can be derived using perturbation theory, where a change in energy can be treated as perturbation, and takes into account the conservation laws physical properties, such as the angular momentum of the system as basis for the selection rules.

The transition's radiation type can be of two main flavors, Electric, E_k , or Magnetic, M_k ,

with k representing its multiplicity. These labels indicate which of the [Electromagnetic Field \(EMF\)](#) component had the strongest influence on the transition's occurrence. For both these types of transitions, the system's total angular momentum is allowed a change of $\Delta J = 0, \pm k$, and so does its projection, M_J . However, different transitions lead to different changes of parity in the system and to different selection rules.

It should also be of note that, usually, for the same multiplicity, an E transition is more intense than an M , and that it is also possible for rare 2-photon transitions to take place, where a combination of different transition types can occur.

The intensity of a transition is proportional to the squared norm of the perturbation's matrix element involving the initial and final state ($\Gamma_{if} \propto |\langle \psi_i | H' | \psi_f \rangle|^2$). It should also be noted that the electron's initial state population will serve as a scaling factor for the transitions' rate. For example, while the transition rate for a $2p_{1/2} \rightarrow 1s$ and $2p_{3/2} \rightarrow 1s$ should be about the same, the orbital $2p_{3/2}$ has double the population $2p_{1/2}$ has, hence why the K_{α_2} line has about half the K_{α_1} line's intensity.

One should also mention that monochromatic transitions do not exist. While the transition might have a well-defined energy, calculated by the difference in energy between the initial and final levels, due to Heisenberg's uncertainty principle, $\Delta E \Delta t > \frac{\hbar}{2}$, there will exist a natural energy broadening, the transition's natural width. The shapes representing these transitions are given by a Lorentzian distribution.

1.3 Solving the atomic many-body problem

When studying a system composed of multiple charged bodies, one must consider all the existing interactions. Whilst there are known analytical solutions for 2-bodies Hydrogenoid systems, with the presence of more non spatially-bound particles, the Coulomb interaction pairs lead to the impossibility of finding a set of analytical wavefunctions which are a part of the Hamiltonian's eigenset. Consecutively, the need for a numerical method that is able to compute solutions for these complex systems arose.

1.3.1 The non-relativistic Hamiltonian

The first approach used in order to solve the many-bodies problem used a non-relativistic consideration. This way, the Hamiltonian consists on the sum of the system's non-relativistic momentum-related energies and the energy of Coulomb interactions between all the bodies in the system, while considering the nucleus as fixed in space, due to it being thousands of times more massive than the orbiting electrons.

Essentially, and in atomic units:

$$\underbrace{\sum_i^N \left(\overbrace{\frac{1}{2} \nabla_i^2}^{E_1} - \overbrace{\frac{Z}{r_i}}^{E_2} \right)}_{\text{Individual Hamiltonian}} + \underbrace{\sum_{i < j}^j \frac{1}{r_{ij}}}_{\text{Pair repulsion}} \quad E_3$$

$$E_1 \rightarrow \text{Momentum} \quad E_2 \rightarrow e^- \text{ nuc. Coulomb attraction} \quad E_3 \rightarrow e^- e^- \text{ Coulomb repulsion} \quad (1.1)$$

1.3.2 The Hartree-Fock Method

This numerical method is one of the staple and most enduring procedures for solving the problem associated with a many-body system. As a side note, an in-depth explanation on all the intricacies of this method can be found in many of the literature, but as for the writing of this thesis, the works [3–6] were the ones consulted.

Hartree developed an iterative method, further enhanced by Fock and Slater, based on the field's [self consistency method](#). In this approach, when studying a multi-electronic system, such as an atom, each electron's wavefunction is composed as a product of a spacial part, ψ , and one related to the electron's spin, χ , as to be able to account for Pauli's exclusion principle and, if so desired, relativistic effects.

$$u = \psi \chi \quad (1.2)$$

The wavefunction capable of describing the whole system, Ψ , should be somewhat of a product of all the wavefunctions describing each individual electron. However, one must not forget the need for this wavefunction to respect the antisymmetry principle, due to the electron's fermionic nature. In order to achieve this, Ψ is to be composed of a Slater determinant:

$$\Psi = \frac{1}{\sqrt{N!}} \begin{vmatrix} u_1(x_1) & u_2(x_1) & \cdots & u_N(x_1) \\ u_1(x_2) & u_2(x_2) & \cdots & u_N(x_2) \\ \vdots & \vdots & \ddots & \vdots \\ u_1(x_N) & u_2(x_N) & \cdots & u_N(x_N) \end{vmatrix} \quad (1.3)$$

Explain anti-symmetry and put it in the glossary

Explain in the glossary

It is of high importance that the set of basis wavefunctions respects orthonormality. These are to be initialized as trial wavefunctions for the numerical method.

The main goal for this algorithm is to, as per the [self consistency method](#), follow the variational principle with the goal of minimize a functional, as a way of reaching an energetic minimum. This optimal, yet unknown energy, E_0 (calculated by operating the Hamiltonian on the system's optimal wavefunctions), will attempt to be reached by the variation of the trial wavefunctions that provide a non-minimized solution. Whilst the optimal wavefunctions will never be reached, the purpose of this method is to reach a

solution that yields an energetic value as close as possible to E_0 , while always yielding $\langle \Psi | H | \Psi \rangle \geq E_0$, due to the numerical nature of the method.

The computational method consists on starting with the previously mentioned trial wavefunctions and employing them in the Hartree-Fock's potential calculation through the [Hartree-Fock \(HF\)](#) equations.

In an over-simplistic scheme, the self-consistent Hartree-Fock computational method can be represented by the block diagram in Figure 2.1.

Finish the explanation

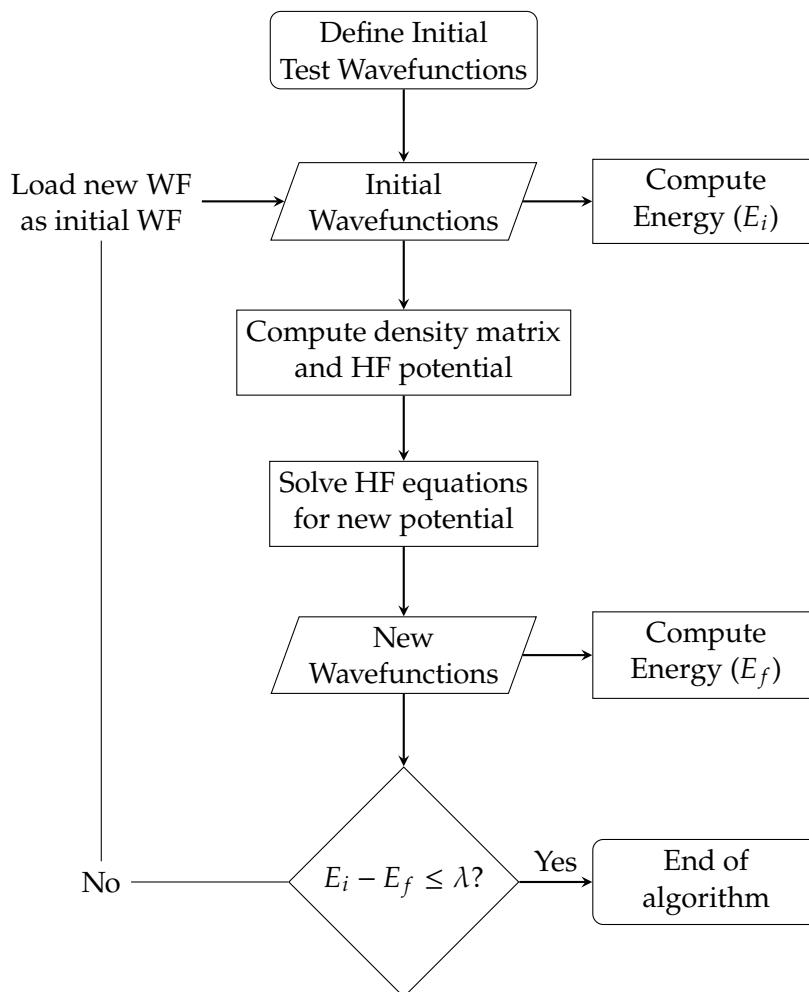


Figure 1.4: HF method's block diagram.

1.3.3 The Dirac Equation

While Schrödinger's equation may be one of the most significant and impactful equations in Modern Physics, it is also not free of its limitations. The fact that it does not account for the existence of the electron's spin and the lack of consideration of relativistic effects are some of the most impactful setbacks. Consulting the works in [7–10], this work will follow an exploration of different approaches that followed in order to solve the aforementioned problem.

Many scientists, such as Klein, Gordon and later Fock, had already conceived a relativistic correction to Schrödinger's equation, where the free-particle energy makes use of the relativistic momentum-energy relation, as displayed in equation (2.4).

$$E = \sqrt{c^2 \mathbf{p}^2 + m^2 c^4} \quad (1.4)$$

This notable definition can be derived from the Lorentz invariant scalar produced by Minkowski norm of the momentum four-vector (2.5).

$$p^\mu p_\mu = m^2 c^2 \Leftrightarrow \frac{E^2}{c^2} - \mathbf{p}^2 = m^2 c^2 \Leftrightarrow \frac{E^2}{c^2} = \mathbf{p}^2 + m^2 c^2 \quad (1.5)$$

Now, inputting this new energy operator into Schrödinger's equation, yields the Klein-Gordon equation (2.6), allowing for Schrödinger's equation to now be Lorentz-invariant (proof can be found in Strickland's book [11]).

$$-\hbar^2 \frac{\partial^2}{\partial t^2} \psi = (-c^2 \hbar^2 \nabla^2 + m^2 c^4) \psi \quad (1.6)$$

This new approach was, however, still limited, as it only described spin 0 particles (e.g., some mesons), and made use of a second order derivative in the time-like component.

Came 1928 and a new equation was developed by Paul Dirac [12], one taking now into account not the classical 3 dimensional space components, but the relativistic four components.

Dirac started by rewriting the energy-momentum relation, ending up with an equivalent equation (2.7), employing 4×4 matrices, due to the 4 relativistic dimensions at play, and incorporating spins into the equation by making use of the Pauli matrices (2.9).

$$E = c \boldsymbol{\alpha} \cdot \mathbf{p} + \beta m c^2, \quad \boldsymbol{\alpha} = (\alpha_1, \alpha_2, \alpha_3) \quad (1.7)$$

$$\alpha_i = \begin{pmatrix} 0 & \sigma_i \\ \sigma_i & 0 \end{pmatrix} \quad \beta = \begin{pmatrix} I_2 & 0 \\ 0 & -I_2 \end{pmatrix} \quad I_2 = \begin{pmatrix} 1 & 0 \\ 0 & 1 \end{pmatrix} \quad (1.8)$$

$$\sigma_1 = \begin{pmatrix} 0 & 1 \\ 1 & 0 \end{pmatrix} \quad \sigma_2 = \begin{pmatrix} 0 & -i \\ i & 0 \end{pmatrix} \quad \sigma_3 = \begin{pmatrix} 1 & 0 \\ 0 & -1 \end{pmatrix} \quad (1.9)$$

In order to fully comprehend this shift of notation, one should equate the square of the two equations, (2.4) and (2.7), and confirm its validity.

$$c^2 \mathbf{p}^2 + m^2 c^4 = c^2 \boldsymbol{\alpha}^2 \mathbf{p}^2 + 2 m c^3 \boldsymbol{\alpha} \cdot \mathbf{p} + \beta^2 m^2 c^4 \quad (1.10)$$

In order for this equation to make sense, the following conditions must be true (which in fact, they are):

Try to explain why this might be a problem

do the demonstration, dummy

$$\begin{cases} c^2 p^2 = c^2 \alpha^2 p^2 & \Leftrightarrow \alpha^2 = 1 \\ 0 = 2mc^3 p \alpha \beta & \Leftrightarrow \alpha \beta = 0 \\ m^2 c^4 = \beta^2 m^2 c^4 & \Leftrightarrow \beta^2 = 1 \end{cases} \quad (1.11)$$

Taking the previous considerations into account, one can now construct Dirac's free-particle equation (2.12):

$$i\hbar \frac{\partial}{\partial t} \psi = (c \alpha \cdot p + \beta mc^2) \psi = \begin{pmatrix} mc^2 I_2 & -i\hbar c \sigma \cdot \nabla \\ -i\hbar c \sigma \cdot \nabla & -mc^2 I_2 \end{pmatrix} \cdot \begin{pmatrix} \psi_1 \\ \vdots \\ \psi_4 \end{pmatrix} \quad (1.12)$$

This equation, however, as mentioned above, can only describe a single particle present in a field-free region. In order to account for the existence of a field, such as the electromagnetic field, derived from the four-potential A^μ , composed by the electric scalar potential field, $A^0 = \phi$, and the vector potential, $(A^1, A^2, A^3) = \mathbf{A}$, the following change on the momentum four-vector must be made:

$$p^\mu \rightarrow p^\mu - eA^\mu, \quad A^\mu = (\phi, \mathbf{A}) \quad (1.13)$$

The Hamiltonian can now be rewritten as to account for the presence of the electromagnetic field (2.14). This way it is possible to include, for example, the electron-nucleus Coulomb attraction.

$$H_D = -e\phi + \beta mc^2 + \alpha(cp + eA) \quad (1.14)$$

For a central fixed potential, as is the one generated by the nuclear charge, the 3 space-like components from the four-potential are null, and the time-like component, $\phi = \frac{Ze}{r}$. The Hamiltonian gains now a more recognizable form:

$$H_D = -\frac{e^2 Z}{r} + \beta mc^2 + \alpha \cdot pc \quad (1.15)$$

A very interesting fact about Dirac's equation is that it yields, in fact, two sets of solutions: the large component (positive energy values), for particles, and the small component (negative energy values), for antiparticles.

1.3.3.1 The Dirac-Breit Equation

Once again, when considering a system composed of many bodies, one must consider all the present interactions, namely, the electron-electron repulsion in an atom. Breit, in 1929, had created a relativistic approach to treat the electron-electron interactions, consisting on a set of equations building upon the classical non-relativistic Hamiltonian from equation (2.1), which can be consulted in Appendix A. Breit's equations are able to

account for angular momenta couplings and estimate level energy splittings, the change of a particle's apparent mass as a function of velocity, and even include the interaction of an applied external magnetic field [10].

It is quite obvious Breit's equations introduce a great complexity in the search of the new Hamiltonian's eigenfunctions. Nonetheless, when trying to include an approximation of Breit's considerations into Dirac's equation, one must add the following operator to the one present in equation (2.15):

$$H_B = \sum_{i>j} \frac{e^2}{r_{ij}} - e^2 \left(\frac{\alpha_i \alpha_j}{r_{ij}} + \frac{(\alpha_i \nabla_i)(\alpha_j \nabla_j) r_{ij}}{2} \right) \quad (1.16)$$

This set of terms will account for the fact that Coulomb interactions, mediated by the electric field, and therefore, **virtual photons**, cannot occur at instantaneous velocities, but at the speed of light.

1.4 QED considerations

Lorem ipsum dolor sit amet, consectetur adipiscing elit. Etiam ut justo justo. Cras pulvinar massa sollicitudin ligula faucibus, in vulputate magna viverra. Nulla risus ante, maximus ut nunc sit amet, condimentum convallis mi. Phasellus et mi aliquet, ornare sapien egestas, vehicula orci. Donec ac massa tempus, iaculis tortor vitae, tempus tortor. Donec nec justo eros. Sed mauris purus, facilisis eu tempus quis, mattis et erat. Sed et congue metus, in venenatis nibh. Nullam ipsum ex, scelerisque non nunc sit amet, ultrices commodo felis. Proin sodales turpis nulla, quis tincidunt leo auctor id. Ut ac nulla quis felis molestie ullamcorper. Nulla tristique dui velit, sit amet rutrum libero dignissim id.

In hac habitasse platea dictumst. Vivamus laoreet neque odio, vitae faucibus massa eleifend sit amet. Curabitur tempor facilisis velit, eget blandit nisi rutrum at. Morbi a massa a lacus lobortis ultricies eget vel enim. Ut augue nisl, tristique eget luctus eget, scelerisque vitae risus. Aliquam in felis et metus euismod porttitor. Nullam nec ligula mi. Aliquam non vulputate sem. Proin ut leo eget ex bibendum venenatis ac vel sapien. Cras felis eros, cursus quis dolor posuere, scelerisque tempus orci. In nec quam in dui efficitur aliquam vitae sit amet dui. Cras laoreet tellus vel risus molestie mattis. Nulla facilisi. Duis rutrum mauris vitae malesuada consequat.

Should the atomic system be subjected to an external **EMF**, the level structure would change due to Zeeman's and Stark's effects, allowing for the probing of the atom's hyperfine structure.

1.4.1 The **MCDF** Method

As previously mentioned in section 2.1.1, there is a need for a numerical method in order to compute and find the eigenfunctions for a many-body Hamiltonian. While the Hartree-Fock method was able to reasonably solve the non-relativistic problem, now,

Falar aqui sobre as contribuições. Não tem que ser extensivo

Ler bem o manual e explicar bem o método e todas as coisas diferentes que se podem fazer

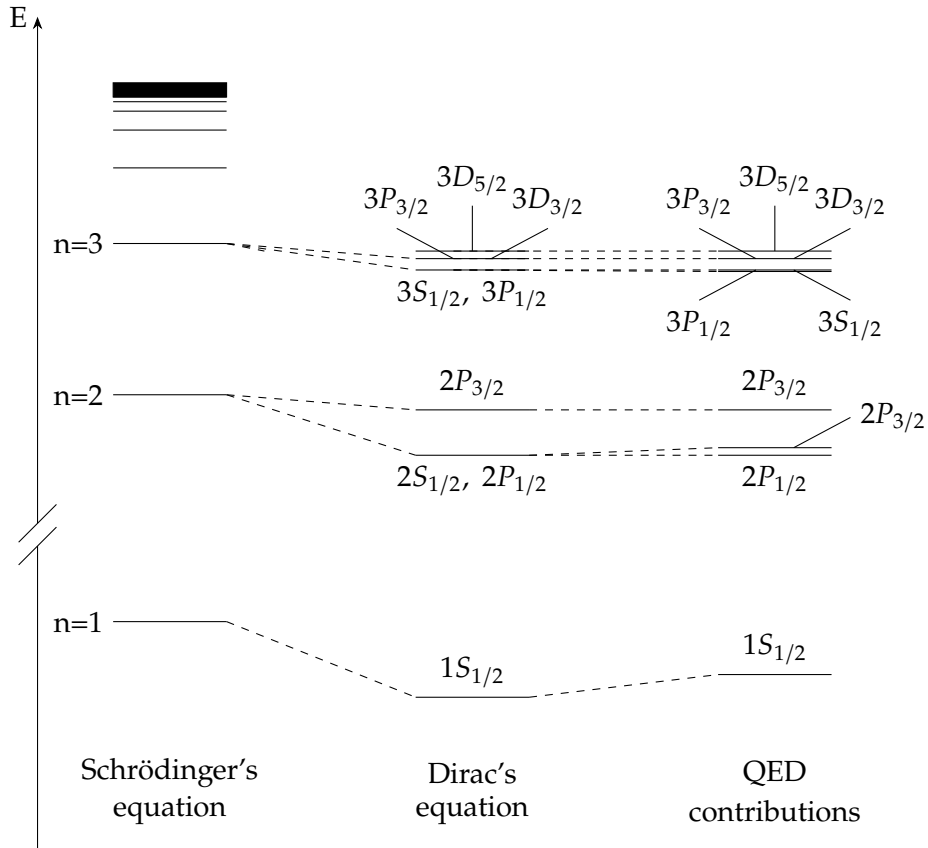


Figure 1.5: Comparison of Hydrogen level diagrams. Adapted from [13]

while considering the Dirac-Breit Hamiltonian from equations (2.15) and (2.16), there is a need for a new method.

Hence, the state of the art *MCDFGME* arises. This self-consistent iterative method, based on the same method present in section 2.1.1, is able to solve and find eigenfunctions for a multielectronic system, now taking into account the Dirac-Breit Hamiltonian. Moreover, it is also capable of incorporating electron correlation and many QED effects not yet considered in the relativistic equation, such as the Lamb-shift, vacuum polarization, and the electron's self energy. A brief description of these contributions can be found in appendix C

1.5 State of the Art

This really needs a re-do

1.5.1 Copper's characteristic X-rays

Copper is a dominant element in today's society. While most of its uses are day-to-day related, it also has a high prevalence in many physical areas, namely, copper's K_α transitions [14]. While these radiative transitions have been measured countless times, with very well recorded energy values [15–19]. It is also common knowledge Copper's K_α

lines do not have a symmetric distribution, since both K_{α_1} and K_{α_2} line display a negative (left-tailed) skewness. Due to this fact, most of the fitting models used in order to analyze both Copper's K_{α_1} and K_{α_2} transitions involve the usage of a Lorentzian doublet, for each line [20, 21]. While many associate these asymmetries due to satellite states formed by shake processes [14, 22], with some theoretical studies having been performed [23], some authors note it could be due to X-ray resonant Raman scattering [22]. This effect occurs when a sample is exposed to energies under to near the ionization threshold, when a bound electron is excited to an upper state [24]. While there are some studies exploring this topic, most are focused on the cascade of low energy transitions that follow the post-scattering excitation [25]. Nonetheless, a previous experimental study has been able to show that for Copper exposed to synchrotron radiation tuned to energies near K-shell's ionization energy, some K_{α_1} transitions demonstrated to be narrower than expected [26].

1.5.2 MCDFGME capabilities

It has been noted multiple times that *MCDFGME* code excels in atomic structure calculations of super-heavy elements and highly-charged ions, where relativistic and QED effects are in prevalence [27–29]. However, it has also been proven to be an excellent tool for the calculation of less ionized and lighter atomic systems [30].

In addition, the *MCDFGME* code is able to calculate radiative and auger transition rates for the calculated configurations, which can be used in the simulation of theoretical spectra, due to being able to compute the transition's intensity and natural width. Since it is able to perform calculations, even for exotic atoms, it can be used to further understand many QED phenomena, further exploring the limits of our theory, and it's comparison to experimental data [31].

It should also be of note that there are many other code alternatives. While *MCDFGME*, which is a close-source project, provides a very high precision in the performed calculations at a high computational cost, *Flexible Atomic Code (FAC)*, is an open source code which requires less computational time for the calculations, however, it lacks *MCDFGME*'s precision, since it only is able to consider all the spin-orb couplings, but does not mix the possible configurations originating them. It can, however, calculate other collisional processes, such as electronic impact excitation cross-sections [32]. *General-purpose Relativistic Atomic Structure Package 2k (Grasp2k)* [33], and *AUTOSTRUCTURE* [34] are other codes with some of the same capabilities.

Atomic Structure Calculations

When studying a system composed of multiple charged bodies, one must consider all the existing interactions. Whilst there are known analytical solutions for the 2-bodies Hydrogenoid systems, with the presence of more non spatially-bound particles, these become impossible to find for Schrödinger's equation, even using Born-Oppenheimer's approximation, where the nucleus is considered static, at a fixed position, making the electrons the only non spatially-bound particles in the system. That way, there was a need for the development of numerical solutions to solve this problem.

2.1 The non-relativistic Hamiltonian

The first approach used in order to solve the many-bodies problem used a non-relativistic consideration. This way, the Hamiltonian consisted on the sum of the system's non-relativistic momentum-related energies and the Coulomb interactions between bodies, while still considering the Born-Oppenheimer approximation.

Essentially, and in atomic units:

$$\underbrace{\sum_i^N \left(\overbrace{\frac{1}{2} \nabla_i^2}^{E_1} - \overbrace{\frac{Z}{r_i}}^{E_2} \right)}_{\text{Individual Hamiltonian}} + \underbrace{\sum_{i < j}^j \overbrace{\frac{1}{r_{ij}}}^{E_3}}_{\text{Pair repulsion}}$$

$$E_1 \rightarrow \text{Momentum} \quad E_2 \rightarrow e^- \text{ nuc. Coulomb attraction} \quad E_3 \rightarrow e^- e^- \text{ Coulomb repulsion} \quad (2.1)$$

2.1.1 The Hartree-Fock Method

Note: This section used the works in [3–6] as reference.

Hartree developed an iterative method, further enhanced by Fock and Slater, based on the field self-consistency method.

In this method, while studying a multi-electronic system, such as an atom, each electron's wavefunction is composed as a product of a spacial part, ψ , and one indicating the electron's spin, χ , as to be able to account for relativistic effects.

$$u = \psi\chi \quad (2.2)$$

The wavefunction capable of describing the whole system, Ψ , should be somewhat of a product of all the wavefunctions describing each individual electron. However, one must not forget the need for this wavefunction to respect the antisymmetry principle, due to the electron's fermionic nature. In order to respect this, Ψ is to be composed of a Slater determinant:

$$\Psi = \frac{1}{\sqrt{N!}} \begin{vmatrix} u_1(x_1) & u_2(x_1) & \cdots & u_N(x_1) \\ u_1(x_2) & u_2(x_2) & \cdots & u_N(x_2) \\ \vdots & \vdots & \ddots & \vdots \\ u_1(x_N) & u_2(x_N) & \cdots & u_N(x_N) \end{vmatrix} \quad (2.3)$$

It is of high importance that the wavefunctions must form an orthonormal basis. These are to be initialized as trial wavefunctions.

The main goal of this method is to follow the variational principle and to minimize a functional, with the purpose of minimizing the system's energy. This optimal, yet unknown energy, E_0 (calculated by Operating the Hamiltonian on the optimal wavefunctions), will try to be reached by varying the trial functions that provide a non-minimized solution, with $\langle \Psi | H | \Psi \rangle \geq E_0$.

The computational method consists on starting with the previously mentioned trial wavefunctions, using them to calculate Hartree-Fock's potential through the HF equations.

In a very simplified way, the self-consistent Hartree-Fock computational method can be represented by the block diagram in Figure 2.1.

2.2 The Dirac Equation

Note: This section used the works in [7–10] as reference.

It is no secret that the Schrödinger equation has some very considerable limitations. The fact that it does not account for the existence of the electron's spin and the lack of consideration of relativistic effects are some of the most impactful setbacks.

Many scientists, such as Klein, Gordon and later Fock, had already conceived a relativistic correction to Schrödinger's equation, where the free-particle energy makes use of the relativistic momentum-energy relation (2.4).

$$E = \sqrt{c^2 p^2 + m^2 c^4} \quad (2.4)$$

Which can be derived from the [Lorentz invariant Minkowski norm](#) of the momentum four-vector (2.5).

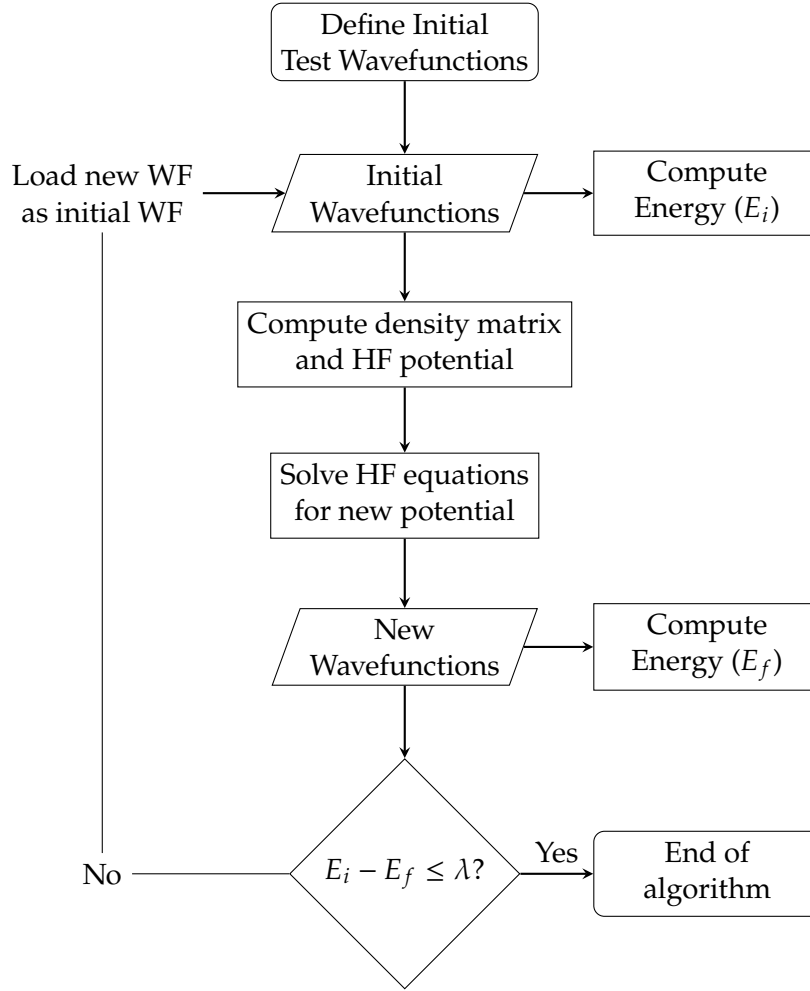


Figure 2.1: HF method's block diagram.

$$p^\mu p_\mu = m^2 c^2 \Leftrightarrow \frac{E^2}{c^2} - \mathbf{p}^2 = m^2 c^2 \Leftrightarrow \frac{E^2}{c^2} = \mathbf{p}^2 + m^2 c^2 \quad (2.5)$$

Now, inputting this new energy operator into Schrödinger's equation, yields the Klein-Gordon equation (2.6), allowing for Schrödinger's equation now to be Lorentz-invariant.

$$-\hbar^2 \frac{\partial^2}{\partial t^2} \psi = \left(-c^2 \hbar^2 \nabla^2 + m^2 c^4 \right) \psi \quad (2.6)$$

This new approach was, however, still faulty, due to only describing spin 0 particles (e.g., some mesons), and making use of a second order derivative in the time-like component.

That way, a new equation was developed by Paul Dirac, in 1928 [12], one taking into account not the classical 3 dimensional space components, but the relativistic four components.

Dirac took a spin at rewriting the energy-momentum relation, ending up with an equivalent equation (2.7), involving 4×4 matrices, due to the 4 relativistic dimensions at play, and incorporating spins into the equation by making use of the now famous Pauli matrices (2.9).

$$E = c\boldsymbol{\alpha} \cdot \mathbf{p} + \beta mc^2, \quad \boldsymbol{\alpha} = (\alpha_1, \alpha_2, \alpha_3) \quad (2.7)$$

$$\alpha_i = \begin{pmatrix} 0 & \sigma_i \\ \sigma_i & 0 \end{pmatrix} \quad \beta = \begin{pmatrix} I_2 & 0 \\ 0 & -I_2 \end{pmatrix} \quad I_2 = \begin{pmatrix} 1 & 0 \\ 0 & 1 \end{pmatrix} \quad (2.8)$$

$$\sigma_1 = \begin{pmatrix} 0 & 1 \\ 1 & 0 \end{pmatrix} \quad \sigma_2 = \begin{pmatrix} 0 & -i \\ i & 0 \end{pmatrix} \quad \sigma_3 = \begin{pmatrix} 1 & 0 \\ 0 & -1 \end{pmatrix} \quad (2.9)$$

In order to fully comprehend this shift of notation, one should equate the square of the two equations, (2.4) and (2.7), and confirm if logic still stands.

$$c^2 \mathbf{p}^2 + m^2 c^4 = c^2 \boldsymbol{\alpha}^2 \mathbf{p}^2 + 2mc^3 \boldsymbol{\alpha} \cdot \mathbf{p} \cdot \beta + \beta^2 m^2 c^4 \quad (2.10)$$

In order for this equation to make sense, the following conditions must be true (which in fact, they are):

$$\begin{cases} c^2 \mathbf{p}^2 = c^2 \boldsymbol{\alpha}^2 \mathbf{p}^2 & \Leftrightarrow \boldsymbol{\alpha}^2 = 1 \\ 0 = 2mc^3 \boldsymbol{\alpha} \cdot \mathbf{p} \cdot \beta & \Leftrightarrow \boldsymbol{\alpha} \beta = 0 \\ m^2 c^4 = \beta^2 m^2 c^4 & \Leftrightarrow \beta^2 = 1 \end{cases} \quad (2.11)$$

With all the previous considerations taken into account, one can now construct Dirac's free-particle equation(2.12):

$$i\hbar \frac{\partial}{\partial t} \boldsymbol{\psi} = (c\boldsymbol{\alpha} \cdot \mathbf{p} + \beta mc^2) \boldsymbol{\psi} = \begin{pmatrix} mc^2 I_2 & -i\hbar c \boldsymbol{\sigma} \cdot \nabla \\ -i\hbar c \boldsymbol{\sigma} \cdot \nabla & -mc^2 I_2 \end{pmatrix} \cdot \begin{pmatrix} \psi_1 \\ \vdots \\ \psi_4 \end{pmatrix} \quad (2.12)$$

This equation, however, as mentioned above, can only describe a single particle present in a field-free region. In order to account for the existence of a field, such as the electromagnetic field, derived from the four-potential A^μ , composed by the electric scalar potential field, $A^0 = \phi$, and the vector potential, $(A^1, A^2, A^3) = \mathbf{A}$, the following change to the momentum four-vector must be made:

$$p^\mu \rightarrow p^\mu - eA^\mu, \quad A^\mu = (\phi, \mathbf{A}) \quad (2.13)$$

The Hamiltonian can now be rewritten to account for the presence of the electromagnetic field (2.14). This way it is possible to include, for example, the electron-nucleus Coulomb attraction.

$$H_D = -e\phi + \beta mc^2 + \boldsymbol{\alpha}(c\mathbf{p} + e\mathbf{A}) \quad (2.14)$$

For a central potential, as is the one generated by the nuclear charge (assuming Born-Oppenheimer's approximation), the 3 space-like components from the four-potential

are null, and the time-like component, $\phi = \frac{Ze}{r}$. The Hamiltonian gains now a more recognizable form:

$$H_D = -\frac{e^2 Z}{r} + \beta mc^2 + \boldsymbol{\alpha} \cdot \mathbf{p}c \quad (2.15)$$

Something very interesting about Dirac's equation is the fact that it does not yield a single solution, but in fact, two: the large component (positive energy values), for particles, and the small component (negative energy values), for antiparticles.

2.3 The Dirac-Breit Equation

Once again, when considering a system composed of many bodies, one must consider all the present interactions, namely, the electron-electron repulsion in an atom. Breit, in 1929, had created a relativistic approach to treat the electron-electron interactions, consisting on a set of equations building upon the classical non-relativistic Hamiltonian from equation (2.1), which can be consulted in Appendix A. Breit's equations are able to account for angular momenta couplings and estimate level energy splittings, the change of a particle's apparent mass as a function of velocity, and even include the interaction of an applied external magnetic field [10].

It is quite obvious Breit's equations introduce a great complexity in the search of the new Hamiltonian's eigenfunctions. However, when trying to include an approximation of Breit's considerations into Dirac's equation, one must add the following operator to the one present in equation (2.15):

$$H_B = \sum_{i>j} \frac{e^2}{r_{ij}} - e^2 \left(\frac{\boldsymbol{\alpha}_i \boldsymbol{\alpha}_j}{r_{ij}} + \frac{(\boldsymbol{\alpha}_i \nabla_i)(\boldsymbol{\alpha}_j \nabla_j) r_{ij}}{2} \right) \quad (2.16)$$

This set of terms will account for the fact that Coulomb interactions, mediated by the electric field, and therefore, **virtual photons**, cannot occur at instantaneous velocities, but at the speed of light.

2.4 The *MCDF* Method

As previously mentioned in section 2.1.1, there is a need for a numerical method in order to compute and find the eigenfunctions for a many-body Hamiltonian. While the Hartree-Fock method was able to reasonably solve the non-relativistic problem, now, while considering the Dirac-Breit Hamiltonian from equations (2.15) and (2.16), there is a need for a new method.

Hence, the state of the art *MCDFGME* arises. This self-consistent iterative method, based on the same method present in section 2.1.1, is able to solve and find eigenfunctions for a multielectronic system, now taking into account the Dirac-Breit Hamiltonian. Moreover, it is also capable of incorporating electron correlation and many QED effects not

yet considered in the relativistic equation, such as the Lamb-shift, vacuum polarization, and the electron's self energy. A brief description of these contributions can be found in [appendix C](#)

Bibliography

- [1] T. D. Thomas. “Transition from Adiabatic to Sudden Excitation of Core Electrons”. In: *Phys. Rev. Lett.* 52 (6 1984), pp. 417–420. DOI: [10.1103/PhysRevLett.52.417](https://doi.org/10.1103/PhysRevLett.52.417). URL: <https://link.aps.org/doi/10.1103/PhysRevLett.52.417> (cit. on p. 4).
- [2] M. F. Vitha, R. Klockenkämper, and A. V. Bohlen. *Chemical Analysis: A Series of Monographs on Analytical Chemistry and Its Applications Total-Reflection X-ray Fluorescence Analysis and Related Methods*. 2nd Edition. Vol. 181. 2015, pp. 20–21 (cit. on pp. 5, 26).
- [3] *Hartree Fock method: A simple explanation*. URL: <https://insilicosci.com/hartree-fock-method-a-simple-explanation/> (cit. on pp. 7, 14).
- [4] J. P. Santos. *FÍSICA ATÓMICA Apontamentos para a UC FA 2020/21* (cit. on pp. 7, 14).
- [5] R. Gabriel and T. Rosa. *The Hartree-Fock Method* (cit. on pp. 7, 14).
- [6] S. M. Blinder. *Introduction to the hartree-fock method*. 2018-01. DOI: [10.1016/B978-0-12-813651-5.00001-2](https://doi.org/10.1016/B978-0-12-813651-5.00001-2) (cit. on pp. 7, 14).
- [7] B. Thaller. *The Dirac Equation*. Springer Berlin Heidelberg, 1992. DOI: [10.1007/978-3-662-02753-0](https://doi.org/10.1007/978-3-662-02753-0) (cit. on pp. 8, 15).
- [8] H. F. Beyer and V. P. Shevelko. *Introduction to the physics of highly charged ions*. IOP Pub, 2016, pp. 1–361. ISBN: 9781420034097. DOI: [10.1016/S0168-9002\(03\)00733-2](https://doi.org/10.1016/S0168-9002(03)00733-2) (cit. on pp. 8, 15).
- [9] J. J. Sakurai and J. Napolitano. *Modern Quantum Mechanics*. Cambridge University Press, 2020-09. DOI: [10.1017/9781108587280](https://doi.org/10.1017/9781108587280) (cit. on pp. 8, 15).
- [10] H. A. Bethe and E. E. Salpeter. *Quantum Mechanics of One- and Two-Electron Atoms*. Springer US, 1977. DOI: [10.1007/978-1-4613-4104-8](https://doi.org/10.1007/978-1-4613-4104-8) (cit. on pp. 8, 11, 15, 18).
- [11] M. Strickland. *Relativistic Quantum Field Theory, Volume 1*. 2053-2571. Morgan & Claypool Publishers, 2019. ISBN: 978-1-64327-702-8. DOI: [10.1088/2053-2571/ab30cc](https://doi.org/10.1088/2053-2571/ab30cc). URL: <https://dx.doi.org/10.1088/2053-2571/ab30cc> (cit. on p. 9).

- [12] P. A. M. Dirac. "The quantum theory of the electron". In: *Proceedings of the Royal Society of London. Series A, Containing Papers of a Mathematical and Physical Character* 117 (778 1928-02), pp. 610–624. ISSN: 0950-1207. DOI: [10.1098/rspa.1928.0023](https://doi.org/10.1098/rspa.1928.0023) (cit. on pp. 9, 16).
- [13] D. Bank. *Atomic physics at GSI / FAIR:current and future research*. 2023-08 (cit. on p. 12).
- [14] T. V. Nguyen et al. "Theory of copper K_α and K_β diagram lines, satellite spectra, and ab initio determination of single and double shake probabilities". In: *Physics Letters, Section A: General, Atomic and Solid State Physics* 426 (2022-02), p. 127900. ISSN: 03759601. DOI: [10.1016/j.physleta.2021.127900](https://doi.org/10.1016/j.physleta.2021.127900). URL: <https://linkinghub.elsevier.com/retrieve/pii/S0375960121007659> (cit. on pp. 12, 13).
- [15] H. A. Melia et al. "The characteristic radiation of copper K_β including radiative Auger processes". In: *Journal of Physics B: Atomic, Molecular and Optical Physics* 53 (19 2020-10), p. 195002. ISSN: 13616455. DOI: [10.1088/1361-6455/aba3a6](https://doi.org/10.1088/1361-6455/aba3a6). URL: <https://iopscience.iop.org/article/10.1088/1361-6455/aba3a6> (cit. on p. 12).
- [16] H. A. Melia et al. "The characteristic radiation of copper K_α 1,2,3,4". In: *Acta Crystallographica Section A: Foundations and Advances* 75 (3 2019-05), pp. 527–540. ISSN: 20532733. DOI: [10.1107/S205327331900130X](https://doi.org/10.1107/S205327331900130X). URL: <http://www.ncbi.nlm.nih.gov/pubmed/31041908> (cit. on p. 12).
- [17] H. Sorum. "The K_α 1,2 X-ray spectra of the 3d transition metals Cr, Fe, Co, Ni and Cu". In: *Journal of Physics F: Metal Physics* 17 (2 1987-02), pp. 417–425. ISSN: 03054608. DOI: [10.1088/0305-4608/17/2/011](https://doi.org/10.1088/0305-4608/17/2/011) (cit. on p. 12).
- [18] J. Bremer, T. Johnsen, and H. Sørsum. "The Cu K_α 1,2 spectrum as measured with a curved-crystal spectrometer". In: *X-Ray Spectrometry* 11 (3 1982), pp. 149–152. ISSN: 10974539. DOI: [10.1002/xrs.1300110312](https://doi.org/10.1002/xrs.1300110312) (cit. on p. 12).
- [19] M. Deutsch et al. "K and K x-ray emission spectra of copper". In: *Physical Review A* 51 (1 1995-01), pp. 283–296. ISSN: 10502947. DOI: [10.1103/PhysRevA.51.283](https://doi.org/10.1103/PhysRevA.51.283) (cit. on p. 12).
- [20] Y. Ito et al. " K_α 1,2 x-ray linewidths, asymmetry indices, and [KM] shake probabilities in elements Ca to Ge and comparison with theory for Ca, Ti, and Ge". In: *Physical Review A* 94 (4 2016-10), p. 042506. ISSN: 24699934. DOI: [10.1103/PhysRevA.94.042506](https://doi.org/10.1103/PhysRevA.94.042506) (cit. on p. 13).
- [21] H. Berger. "Study of the K_α emission spectrum of copper". In: *X-Ray Spectrometry* 15 (4 1986-10), pp. 241–243. ISSN: 0049-8246. DOI: [10.1002/xrs.1300150405](https://doi.org/10.1002/xrs.1300150405). URL: <https://onlinelibrary.wiley.com/doi/10.1002/xrs.1300150405> (cit. on p. 13).

- [22] S. Galambosi et al. “Near-threshold multielectronic effects in the Cu $K_{\alpha_{1,2}}$ x-ray spectrum”. In: *Physical Review A - Atomic, Molecular, and Optical Physics* 67 (2 2003-02), p. 5. ISSN: 10941622. DOI: [10.1103/PhysRevA.67.022510](https://doi.org/10.1103/PhysRevA.67.022510). URL: <https://link.aps.org/doi/10.1103/PhysRevA.67.022510> (cit. on p. 13).
- [23] C. T. Chantler, A. C. Hayward, and I. P. Grant. “Theoretical Determination of Characteristic X-Ray Lines and the Copper K_{α} Spectrum”. In: *Physical Review Letters* 103 (12 2009-09), p. 123002. ISSN: 00319007. DOI: [10.1103/PhysRevLett.103.123002](https://doi.org/10.1103/PhysRevLett.103.123002). URL: <https://journals.aps.org/prl/abstract/10.1103/PhysRevLett.103.123002> (cit. on p. 13).
- [24] F. Gel'mukhanov and H. Ågren. *Resonant X-ray Raman scattering*. Vol. 312. Elsevier, 1999, pp. 87–330. DOI: [10.1016/S0370-1573\(99\)00003-4](https://doi.org/10.1016/S0370-1573(99)00003-4) (cit. on p. 13).
- [25] P. Carra, M. Fabrizio, and B. T. Thole. “High resolution x-ray resonant Raman scattering”. In: *Physical Review Letters* 74 (18 1995-05), pp. 3700–3703. ISSN: 00319007. DOI: [10.1103/PhysRevLett.74.3700](https://doi.org/10.1103/PhysRevLett.74.3700) (cit. on p. 13).
- [26] P. Eisenberger, P. M. Platzman, and H. Winick. “X-ray resonant Raman scattering: Observation of characteristic radiation narrower than the lifetime width”. In: *Physical Review Letters* 36 (11 1976-03), pp. 623–626. ISSN: 00319007. DOI: [10.1103/PhysRevLett.36.623](https://doi.org/10.1103/PhysRevLett.36.623) (cit. on p. 13).
- [27] P. Indelicato, J. Bieroń, and P. Jönsson. “Are MCDF calculations 101% correct in the super-heavy elements range?” In: *Theoretical Chemistry Accounts* 129 (3-5 2011-06), pp. 495–505. ISSN: 1432881X. DOI: [10.1007/s00214-010-0887-3](https://doi.org/10.1007/s00214-010-0887-3) (cit. on p. 13).
- [28] P. Indelicato, O. Gorgeix, and J. P. Desclaux. “Multiconfigurational Dirac-Fock studies of two-electron ions. II. Radiative corrections and comparison with experiment”. In: *Journal of Physics B: Atomic and Molecular Physics* 20 (4 1987-02), p. 651. ISSN: 0022-3700. DOI: [10.1088/0022-3700/20/4/007](https://doi.org/10.1088/0022-3700/20/4/007) (cit. on p. 13).
- [29] O. Gorgeix, P. Indelicato, and J. P. Desclaux. “Multiconfiguration Dirac-Fock studies of two-electron ions. I. Electron-electron interaction”. In: *Journal of Physics B: Atomic and Molecular Physics* 20 (4 1987-02), pp. 639–649. ISSN: 00223700. DOI: [10.1088/0022-3700/20/4/006](https://doi.org/10.1088/0022-3700/20/4/006) (cit. on p. 13).
- [30] M. Guerra et al. “Fundamental Parameters Related to Selenium K_{α} and K_{β} Emission X-ray Spectra”. In: *Atoms* 9 (1 2021-01), p. 8. ISSN: 2218-2004. DOI: [10.3390/atoms9010008](https://doi.org/10.3390/atoms9010008). URL: <https://www.mdpi.com/2218-2004/9/1/8> (cit. on p. 13).
- [31] N. Paul et al. “Testing Quantum Electrodynamics with Exotic Atoms”. In: *Physical Review Letters* 126 (17 2021-04), p. 173001. ISSN: 10797114. DOI: [10.1103/PhysRevLett.126.173001](https://doi.org/10.1103/PhysRevLett.126.173001) (cit. on p. 13).
- [32] M. F. Gu. *The flexible atomic code*. 2008-05. DOI: [10.1139/P07-197](https://doi.org/10.1139/P07-197) (cit. on p. 13).

- [33] P. Jönsson et al. “New version: Grasp2K relativistic atomic structure package”. In: *Computer Physics Communications* 184 (9 2013-09), pp. 2197–2203. ISSN: 00104655. DOI: [10.1016/j.cpc.2013.02.016](https://doi.org/10.1016/j.cpc.2013.02.016) (cit. on p. 13).
- [34] *ASCL.net - AUTOSTRUCTURE: General program for calculation of atomic and ionic properties*. URL: <https://ascl.net/1612.014> (cit. on p. 13).
- [35] W. E. Lamb and R. C. Retherford. “Fine structure of the hydrogen atom by a microwave method”. In: *Physical Review* 72 (3 1947-08), pp. 241–243. ISSN: 0031899X. DOI: [10.1103/PhysRev.72.241](https://doi.org/10.1103/PhysRev.72.241) (cit. on p. 27).

The Breit Hamiltonian Operators

Note: This operators are valid for the electrons in an atom.

The free particle energy:

$$H_0 = \sum_i^N \frac{p_i^2}{2m_e} \quad (\text{A.1})$$

The electron-nucleus Coulomb attraction:

$$H_1 = \sum_i^N -\frac{e^2 Z}{r_i} \quad (\text{A.2})$$

The electron-electron Coulomb repulsion:

$$H_2 = \sum_{i < j} \frac{e^2}{r_{ij}} \quad (\text{A.3})$$

Incorporates the relativistic apparent mass - velocity dependance:

$$H_3 = -\frac{1}{8m_e^3 c^2} \sum_i^N p_i^4 \quad (\text{A.4})$$

Electric field retardation and magnetic dipole interaction:

$$H_4 = -\frac{e^2}{2m_e^2 c^2} \sum_{i < j} \left[\frac{\mathbf{p}_i \cdot \mathbf{p}_j}{r_{ij}} + \frac{(\mathbf{r}_{ij} \cdot \mathbf{p}_{ij})(\mathbf{r}_{ij} \cdot \mathbf{p}_j)}{r_{ij}^3} \right] \quad (\text{A.5})$$

Darwin's term, accounts for the electron's quantum fluctuation motion:

$$H_5 = \frac{\pi e \hbar^2}{2m_e^2 c^2} \sum_{i < j} \frac{Z}{2} [\delta(\mathbf{r}_i) + \delta(\mathbf{r}_j)] + \delta(\mathbf{r}_{ij}) \quad (\text{A.6})$$

And the last two operators, for the consideration of spin orbit interactions:

$$H_6 = \frac{e^2 \hbar^2}{2m_e^2 c^2} \sum_{i < j} \left(Z \frac{\mathbf{r}_i \times \mathbf{p}_i}{r_i^3} - \frac{\mathbf{r}_{ij} \times \mathbf{p}_i}{r_{ij}^3} + 2 \frac{\mathbf{r}_{ij} \times \mathbf{p}_j}{r_{ij}^3} \right) \mathbf{s}_i + \left(Z \frac{\mathbf{r}_j \times \mathbf{p}_j}{r_j^3} - \frac{\mathbf{r}_{ji} \times \mathbf{p}_j}{r_{ij}^3} + 2 \frac{\mathbf{r}_{ji} \times \mathbf{p}_i}{r_{ij}^3} \right) \mathbf{s}_j \quad (\text{A.7})$$

$$H_7 = \frac{e^2 \hbar^2}{m_e^2 c^2} \sum_{i < j} \left(-\frac{8\pi}{3} \mathbf{s}_i \cdot \mathbf{s}_j \delta(\mathbf{r}_{ij}) + \frac{1}{r_{ij}^3} \left[\mathbf{s}_i \cdot \mathbf{s}_j - \frac{3(\mathbf{s}_i \cdot \mathbf{r}_{ij})(\mathbf{s}_j \cdot \mathbf{r}_{ij})}{r_{ij}^2} \right] \right) \quad (\text{A.8})$$

Transition Diagram

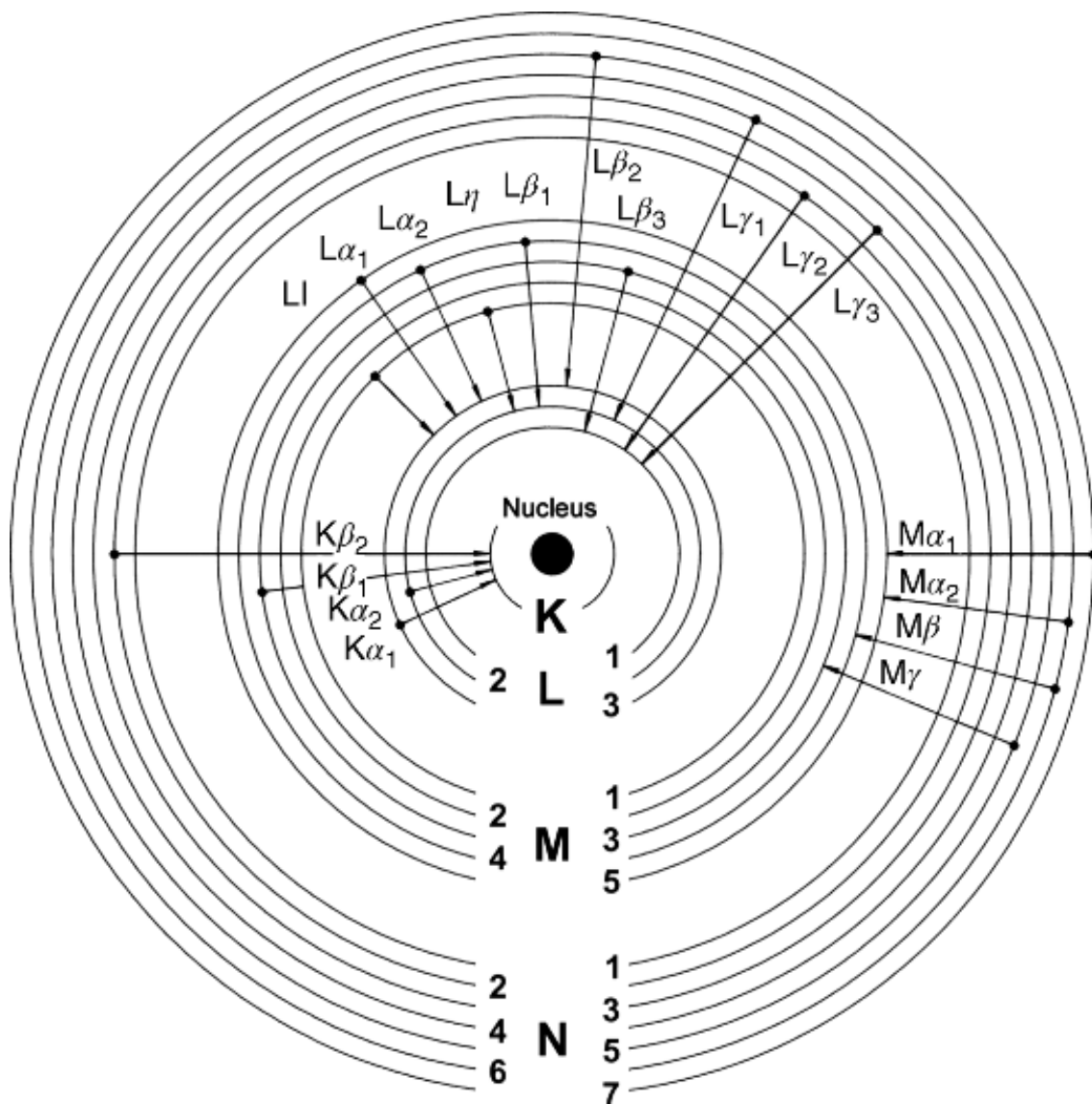


Figure B.1: Transition notation scheme. Adapted from [2]

QED considerations

It should be apparent by now that studying Atomic systems call not only for relativistic effects and corrections, but also for QED ones.

One of the most famous cases where QED came to light was the discovery of the Lamb Shift [35], when it was discovered Hydrogen's $2s_{1/2}$ and $2p_{1/2}$ levels were in fact, not degenerate (did not have the same energy), contrary to what was expected from solving Dirac's equation. This difference in energy came to be known as the Lamb Shift, only explained by QED effects.

C.1 Self-Energy

The self-energy represents a particle's emission and reabsorption of virtual photon, present in the particle's own generated field. This interaction has the most impact in the Lamb Shift effect and when performing energy corrections. One of its [Feynman Diagrams](#) can be seen in Figure C.1a.

C.2 Vacuum Polarization

As previously stated, electromagnetic fields, such as the Coulomb field generated by the nucleus, are mediated by virtual photons. These photons can lead to the creation of electron-positron pairs which create screening effects. Pair annihilation will follow, leading to the production of another virtual photon (Figure C.1b).



Figure C.1: QED Feynman Diagrams

Input File .f05 Example

```

1  program_year=2019 program_version=1
2  * 1 Z=29 (1s)1 (2s)2 (2p)6 (3s)2 (3p)6 (3d)10 (4s)2 2J=1 neig=[2S1/2]#1
   LS1
3      scfmdf max :
4      mod_lightspeed=n
5      nz=29
6      mdf opt_ener=todo modfilename_ener=n modfilename_wf=n do_scf=y
7      Breit=full mag_scf=y ret_scf=y
8      qedstpg_n4=n
9      vacpol_scf=y
10     energy
11     # use_mcdfener=y
12     # opt_relax=y
13     ret_Lorentz=y
14     opt_qedel=y :
15     # ":" above is for ilams taken to be the default value
16     mod_mesh=n
17     # hx=0.012 r(1)=0.001 amesh=0.01 :
18     exotic=n
19     use_nms=y
20     mod_nuc=n
21     project=n
22     # cgt_order_vint=y order=6
23     cgt_order_vint=n
24     def_config=given
25     nbel=29 jjt=1 :
26     c 1 (1s)1 (2s)2 (2p)6 (3s)2 (3p)6 (3d)10 (4s)2 :
27     end
28     # initial state parameters
29     neigv=1 icmul=0 iprfgr=0
30     norbsc=00 ndep=0 nlec=0 nec=1 :
31     nstep=0
32     lregul=n modtest=n
33     modsolv_orb=n
34     mod_odlm=n

```

```
35 # data for uwfrdf
36 :
37 **
```



2023 Year-End Report on Participation in High-Speed Rail

The following table provides a detailed overview of the participation data for the 2023 fiscal year, categorized by region and demographic group. The data is presented in a structured format, allowing for easy comparison and analysis of trends across different segments of the population.

Region	Age Group	Gender	Participation Rate (%)
North America	18-24	Male	75.2
North America	18-24	Female	68.9
North America	25-34	Male	82.1
North America	25-34	Female	76.5
North America	35-44	Male	88.3
North America	35-44	Female	81.7
North America	45-54	Male	91.5
North America	45-54	Female	85.2
North America	55-64	Male	93.8
North America	55-64	Female	87.4
North America	65+	Male	95.1
North America	65+	Female	89.6
Europe	18-24	Male	78.5
Europe	18-24	Female	72.3
Europe	25-34	Male	85.7
Europe	25-34	Female	79.4
Europe	35-44	Male	90.2
Europe	35-44	Female	83.6
Europe	45-54	Male	92.8
Europe	45-54	Female	86.1
Europe	55-64	Male	94.5
Europe	55-64	Female	88.9
Europe	65+	Male	96.2
Europe	65+	Female	90.7
Asia	18-24	Male	81.3
Asia	18-24	Female	75.8
Asia	25-34	Male	87.9
Asia	25-34	Female	81.2
Asia	35-44	Male	92.4
Asia	35-44	Female	85.7
Asia	45-54	Male	95.6
Asia	45-54	Female	88.9
Asia	55-64	Male	97.1
Asia	55-64	Female	91.5
Asia	65+	Male	98.4
Asia	65+	Female	92.8
Africa	18-24	Male	72.6
Africa	18-24	Female	66.1
Africa	25-34	Male	79.8
Africa	25-34	Female	73.2
Africa	35-44	Male	84.5
Africa	35-44	Female	77.9
Africa	45-54	Male	88.7
Africa	45-54	Female	81.3
Africa	55-64	Male	91.2
Africa	55-64	Female	84.8
Africa	65+	Male	93.5
Africa	65+	Female	87.1

The data indicates a general trend of increasing participation rates across all regions and age groups, with higher rates observed in older age groups and in regions with higher population density. The participation rates for males are consistently higher than for females across all categories.

The following table provides a detailed overview of the participation data for the 2023 fiscal year, categorized by region and demographic group. The data is presented in a structured format, allowing for easy comparison and analysis of trends across different segments of the population.

Region	Age Group	Gender	Participation Rate (%)
North America	18-24	Male	75.2
North America	18-24	Female	68.9
North America	25-34	Male	82.1
North America	25-34	Female	76.5
North America	35-44	Male	88.3
North America	35-44	Female	81.7
North America	45-54	Male	91.5
North America	45-54	Female	85.2
North America	55-64	Male	93.8
North America	55-64	Female	87.4
North America	65+	Male	95.1
North America	65+	Female	89.6
Europe	18-24	Male	78.5
Europe	18-24	Female	72.3
Europe	25-34	Male	85.7
Europe	25-34	Female	79.4
Europe	35-44	Male	90.2
Europe	35-44	Female	83.6
Europe	45-54	Male	92.8
Europe	45-54	Female	86.1
Europe	55-64	Male	94.5
Europe	55-64	Female	88.9
Europe	65+	Male	96.2
Europe	65+	Female	90.7
Asia	18-24	Male	81.3
Asia	18-24	Female	75.8
Asia	25-34	Male	87.9
Asia	25-34	Female	81.2
Asia	35-44	Male	92.4
Asia	35-44	Female	85.7
Asia	45-54	Male	95.6
Asia	45-54	Female	88.9
Asia	55-64	Male	97.1
Asia	55-64	Female	91.5
Asia	65+	Male	98.4
Asia	65+	Female	92.8
Africa	18-24	Male	72.6
Africa	18-24	Female	66.1
Africa	25-34	Male	79.8
Africa	25-34	Female	73.2
Africa	35-44	Male	84.5
Africa	35-44	Female	77.9
Africa	45-54	Male	88.7
Africa	45-54	Female	81.3
Africa	55-64	Male	91.2
Africa	55-64	Female	84.8
Africa	65+	Male	93.5
Africa	65+	Female	87.1

The data indicates a general trend of increasing participation rates across all regions and age groups, with higher rates observed in older age groups and in regions with higher population density. The participation rates for males are consistently higher than for females across all categories.